멤브레인(Membrane Journal)
Vol. 29 No. 6 December, 2019, 299-307

총 설

Print ISSN: 1226-0088
Online ISSN: 2288-7253
DOI: https://doi.org/10.14579/MEMBRANE_JOURNAL.2019.29.6.299

전이 금속 산화물을 이용한 가시광선 기반 광촉매 분해

이 수 민* · 박 예 지* · 이 재 훈** · 라즈쿠마 파텔***,†

*연세대학교 융합과학공학부, **연세대학교 화공생명공학과, ***연세대학교 융합과학공학부
(2019년 11월 15일 접수, 2019년 12월 11일 수정, 2019년 12월 16일 채택)

Visible Light-based Photocatalytic Degradation by Transition Metal Oxide

Soomin Lee*, Yeji Park*, Jae Hun Lee, and Rajkumar Patel***,†**

*Nano Science and Engineering, Integrated Science and Engineering Division, Underwood International College, Yonsei University, Yonsei University, 85 Songdogwahak-ro, Yeonsu-gu, Incheon 21983, South Korea
**Department of Chemical and Biomolecular Engineering, Yonsei University, 50 Yonsei-ro, Seodaemun-gu, Seoul 03722, Korea
***Energy Environmental Science and Engineering, Integrated Science and Engineering Division, Underwood International College, Yonsei University, 85 Songdogwahak-ro, Yeonsu-gu, Incheon 21983, South Korea.
(Received November 15, 2019, Revised December 11, 2019, Accepted December 16, 2019)

요 약: 광촉매는 물에서 유기 염료를 분해하는 친환경적 기술이다. 산화 텅스텐은 이산화 티타늄에 비해 더 작은 밴드갭을 지니고 있어 광촉매 나노물질로서 활발히 연구되고 있다. 계층적 구조의 합성, 백금 도핑, 나노 복합물 또는 다른 반도체와의 결합 등이 광촉매 분해 효율을 향상시키는 방법들로 연구되고 있다. 이들 방법들은 광 파장의 적색편이를 유도하여 전자 이동, 전자-정공 쌍의 형성과 재결합에 영향을 미친다. 산화 텅스텐의 형태 개질을 통해 앞서 언급한 광촉매 분해 효율을 향상시키는 방법들과 합성에 대해 분석하였으며 금속 산화물과 탄소 복합재를 결합하는 방법이 새로운 물질의 합성이 필요 없으며 가장 효율적인 방법으로 조사되었다. 이러한 광촉매 기술은 수처리 분리막기술과 모듈화하여 정수처리 목적으로 사용될 수 있다.

Abstract: Photocatalysis is an environment friendly technique for degrading organic dyes in water. Tungsten oxide is becoming an active area of research in photocatalysis nanomaterials for having a smaller bandgap than the previously favored titanium dioxide. Synthesis of hierarchical structures, doping platinum (Pt), coupling with nanocomposites or other semiconductors are investigated as valid methods of improving the photocatalytic degradation efficiency. These impact the reaction by creating a redshift in the wavelength of light used, effecting charge transfer, and the formation/recombination of electron-hole pairs. Each of the methods mentioned above are investigated in terms of synthesis and photocatalytic efficiency, with the simplest being modification on the morphology of tungsten oxide, since it does not need synthesis of other materials, and the most efficient in photocatalytic degradation being complex coupling of metal oxides and carbon composites. The photocatalysis technology can be incorporated with water purification membrane by modularization process and applied to advanced water treatment system.

***Keywords**: photocatalysis, WO_3, organic dye, degradation*

1. Introduction

Conserving the environment is becoming an ever-growing issue as new materials are being synthesized. These new materials have complex structures, making it difficult for them to be decomposed naturally. Using photocatalysis, it is possible to degrade organic dyes under irradiation of light. Transition metal oxides such

†Corresponding author(e-mail: rajkumar@yonsei.ac.kr, https://orcid.org/0000-0002-3820-141X)

as titanium dioxide or tungsten oxide are used for this because their energy levels can allow (i) absorption in the UV and visible light region and (ii) the use of this absorbed energy for reduction of oxygen. Thus, facilitating the decomposition of organic compounds.

Although Titanium dioxide is most widely used in photocatalysis studies, because it has a band gap energy of 3.2 eV (anatase), it functions only in UV light conditions, only being spread into the visible light region when treated with by methods such as doping. Tungsten oxide has the advantage of working better in visible light conditions than titanium dioxide because it has a relatively smaller band gap of 2.4~2.8 eV[1]. This is important because only about 4 to 5% of solar radiation is UV light while approximately 40% is visible light[2].

However, even with the smaller band gap, tungsten oxide does not show a high activity in visible light because the conduction band has an energy level that is higher than the O_2/O_2^- reduction potential[3]. There are various methods to improve the photocatalytic degradation efficiency of tungsten oxide in visible light, with the simplest being changing the morphology of tungsten oxide. Other methods would be using noble metal composites, carbon composites, or coupling with other semiconductors, along with other more complex methods. Here the advantages and disadvantages of each method are examined in more detail.

2. Tungsten Oxide (WO_3)

For most of the recent methods for synthesizing 3D nanostructures from tungsten oxide, a special template is needed[4]. However, such structures can also be achieved without a template in a hydrothermal process where the pH of the precursor solution is modified. The solution consists of $Na_2WO_4 \cdot 2H_2O$, NaCl, HCl mixed in deionized water. In this article, tungsten oxide was fabricated into a 3D architecture consisting of 1D nanorods, which is efficient in degradation of rhodamine B (RhB) under UV-light. Measurements were conducted for samples WO_3-1.5, 2.0, 2.5 and 3.0.

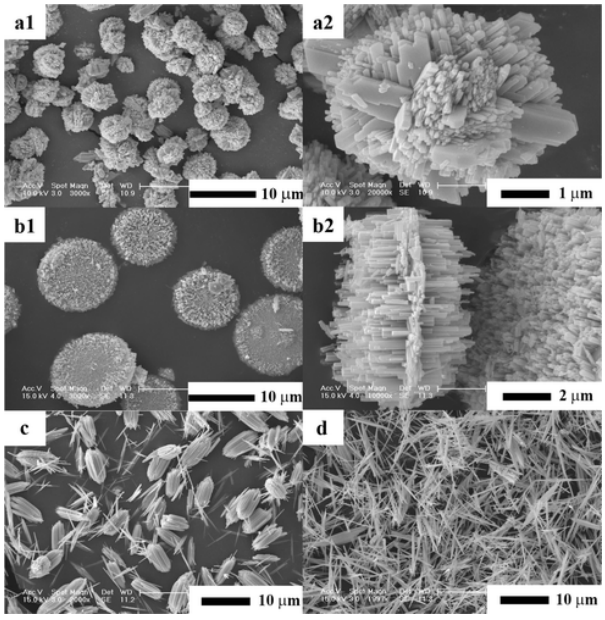

Fig. 1. FESEM images of the as-prepared products synthesized at different pH values of the precursor solution: WO_3-1.5 (a1, a2), WO_3-2.0 (b1, b2), WO_3-2.5 (c), and WO_3-3.0 (d) (Reproduced from Xu *et al.*, 4 with permission of American Chemical Society).

FESEM of the samples with highest photodegradation efficiency, the samples with precursor solution pH of 1.5, showing nanorods with smooth surfaces that make flower-like structures which are 3~5 μm in diameter, and of pH 2.0, showing sandwich structures with two outer layers consisting of a bundle of nanorods, one thin interlayer consisting of horizontal nanorods (Fig. 1). The photodegradation efficiency was tested for RhB in UV-light and divided by the BET surface area, so as to eliminate the effects of surface area and make a comparison based on the effects of photoinduced charges. Photodegradation efficiency of WO_3-1.5 and WO_3-2.0 is higher than WO_3-2.5 and WO_3-3.0. Due to having a partly monoclinic structure, the result for WO_3-1.5 stretched into the range of visible light. WO_3 synthesized at lower pH showed higher charge separation with lower charge carrier recombination resulting in longer life time and higher photocatalytic efficiency. This mechanism can be extended to other areas like the purification of water, gas sensors, and solar energy cells.

2.1. Nanocomposite of noble metal and tungsten oxide

WO_3 is effective as a visible light photocatalyst in the decomposition of organic compounds, especially when loaded with Platinum[5]. While decomposition by WO_3 was believed to be ineffective in air due to the conduction band (CB) level being more positive than the reduction potentials of O_2, because Pt catalyzes the more positive multi-electron reduction of O_2, high efficiency in $PtWO_3$ was observed. A photodeposition method was used to load Pt on WO_3 of particle size 50~200 nm, using $H_2PtCl_6 \cdot 6H_2O$ and visible light irradiation, and resulted in platinum particles of average size 5 nm, uniformly distributed on the surface of WO_3. Nitrogen-doped TiO_2 (N-TiO_2) was prepared as a reference sample. With full-arc irradiation in an aqueous acetic acid (AcOH) solution, Pt-WO_3 showed a higher rate of CO_2 generation than TiO_2 and presented a rate nearly as high as in full-arc for visible light. Comparing the action spectra with the photoabsorption data for pure WO_3 leads to the conclusion that the band gap of WO_3 is responsible for the decomposition. Isopropyl alcohol (IPA) decomposition in the visible light region for WO_3 with an optimal Pt loading (0.5 wt%) showed a 100-fold enhanced CO_2 generation rate (from 0.4 to 48 μmol/h), while for N-TiO_2 with optimal Pt loading showed only a 4-fold increase. Another group reported that when platinum is loaded on WO_3, it acts as a co-catalyst and facilitates multielectron O_2 reduction, improving photodegradation efficiency[6]. WO_3 nanoparticles with an original size of 7.3 ± 1.8 nm was annealed at temperatures 300, 350, 400, 450, 500, 550, and 600°C. The higher the annealing temperature, the larger the resulting particle size. XRD peaks of WO_3 corresponded to the monoclinic phase. A photoreduction technique was used to load WO_3 with Pt. 1 wt% Pt was used because of its activeness in amaranth degradation. Crystallite size, and therefore particle size, grew with higher annealing temperature. Amaranth was used in calculating the rate of photocatalytic activity because it does not degrade under visible light without a photocatalyst. For the amaranth degradation by Pt-WO_3 under visible light when WO_3 particle size range was 18 to 26.4 nm, the initial rate was approximately 3.5 times higher than at 7.3~9.8 and 42.4 nm. Bare WO_3 showed similar tendencies. Pt-WO_3 was 6 times higher than bare WO_3 of same particle size. The initial rate for N-doped TiO_2 was lower than bare WO_3. When particles are at their optimal size of around 19.2 nm, the balance between surface area and surface recombination rate is most optimal. Photoluminescence (PL) spectra indicated that both the recombination of carriers and number of defects are minimum at 500°C where particle size was 19.2 ± 5.4 nm. It was also the most active for the degradation of rhodamine-B.

2.2. Nanocomposite of carbon and tungsten oxide

The graphitic carbon nitride (g-C_3N_4) sheets were synthesized by decomposition of melamine[7]. The synthesis of $W_{18}O_{49}$ nanorods (NRs) involved a solvothermal process including ethanol and heating at 200 °C for 6~8 h. g-C_3N_4/$W_{18}O_{49}$ nanocomposite (NC) was synthesized in a solvothermal process similar to $W_{18}O_{49}$ NRs. The TEM image show a plate shape with pores for g-C_3N_4 sheets. According to HRTEM, few-layered g-C_3N_4 sheets are strongly coupled with well crystallized $W_{18}O_{49}$ NRs of diameter 8~10 nm that are uniformly distributed on them. The g-C_3N_4/$W_{18}O_{49}$ NC showed higher adsorption and photodegradation efficiency for methylene blue (MB) and methyl orange (MO) than for the g-C_3N_4 sheets and $W_{18}O_{49}$ NRs, with a removal efficiency of 99.14% in the dark and 99.91% including photocatalysis in the case of MB. The higher adsorption capacity of $W_{18}O_{49}$ NRs and g-C_3N_4/$W_{18}O_{49}$ NC for MB than g-C_3N_4 is attributed to the existence of unique crystal defects in $W_{18}O_{49}$. While the high photocatalytic efficiency stems from the Z-scheme photocatalytic mechanism operating in heterojunction between the two materials.

Kim *et al.* reported loaded of nanodiamond (ND) powder on WO_3 using dehydration condensation to make ND/WO_3[8]. HR-TEM images show the surface of the ND/WO_3 was covered by ND 2~10 nm in size with a

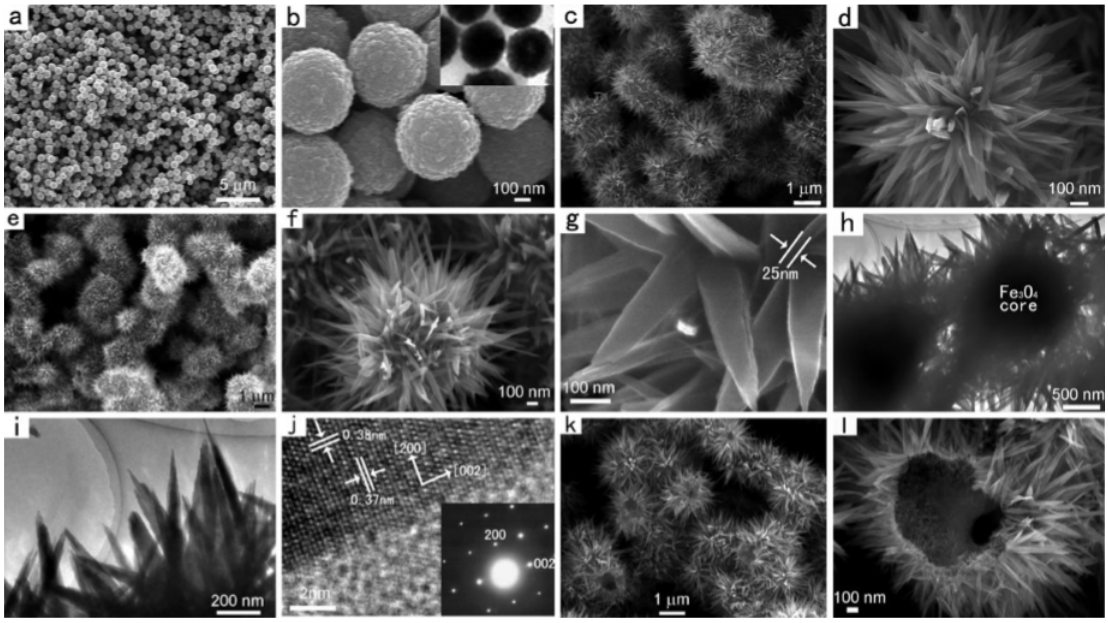

Fig. 2. SEM and TEM images. a, b: Low- and high-magnification SEM images of the Fe_3O_4 microspheres. The inset is a TEM image of the sample. c, d: Low- and high-magnification SEM images of the $Fe_3O_4/W_{18}O_{49}$ core-shell precursors. e-g: Low- and high-magnification SEM images of the Fe_3O_4/WO_3 core-shell structures. h: TEM images of the Fe_3O_4/WO_3 core-shell structures. i: TEM image of the WO_3 nanoplates. j: HRTEM image of the WO_3 nanoplates; the inset is the corresponding SAED pattern. k, l: Low- and high-magnification SEM images of the WO_3 hollow microspheres[14].

carbon layer of thickness ≤ 1 nm on their surfaces. WO_3 showed the highest activity for the visible light photocatalytic degradation of acetaldehyde among various photocatalysts including TiO_2, TaON, C_{60}-TiO_2, TiO_2/WO_3, N-doped TiO_2 (Fig. 2). WO_3 was considerably covered for ND (16 wt%)/WO_3 but only partially covered for ND (8 wt%)/WO_3. Diffuse reflectance UV/visible absorption spectra (DRS) showed insignificant change due to diamond having high transparencies as opposed to other carbon composites such as carbon nanotubes or GO. ND/WO_3 showed a higher efficiency than WO_3 in the visible light photodegradation of organic compounds comparable to Pt/WO_3. NDs function as a co-catalyst, similar to Pt, by facilitating the reduction of O_2. Interfacial electron transfer is enhanced by the sp^2 and sp^3 orbitals each from the shell of graphitic carbon and the diamond core. The photocatalytic activity responds closely to the graphitic layer content and the surface functional groups. Noble metals (e.g. Pt, Pd), often used as a co-catalyst for WO_3 are an expensive type of material, while carbon is one of the most abundant elements on earth. That is why NDs are suggested as an alternative co-catalyst to facilitate visible light photocatalytic purification of air.

Another group used a porous tungsten oxide nanoframework with graphene (GWF) which is a porous tungsten oxide nanoframework with graphene to degrade pollutants under visible light[9]. GWF has significant adsorptivity of aromatic molecules, large range of light absorption, considerable light trapping, and efficiently separated charge carriers. These properties increased the photocatalytic efficiency. Compared to bare WO_3 and TiO_2 nanomaterials, the degradation of Rhodamine B showed a substantial photocatalytic improvement under visible light irradiation. After 15 minutes of visible light irradiation, almost 100% of the Rh B molecules were degraded. However, only 48.6 and 82.3% Rh B were degraded with bare WO_3 nanofibers and TiO_2 under the same condition. This research is important since they used graphene film. It was powder in previous researches that showed significant photocatalytic ability. To overcome the prob-

lem of graphene, it is important to coat on the graphene's surface with WO_3. To synthesis GWF, they used electrospinning technique. After the calcination, we can see the WO_3 nanofibers coated on the graphene from the SEM image and they increased the integrality of the GWF. Also, the TEM image showed the porous surface of GWF. The pores increased the surface area (56.4 m^2g^{-1}) and the photocatalytic ability from the multiple reflection of visible light. Ismail *et al.* compared photodegradation efficiency of Methylene Blue dye using WO_3, WO_3-graphene oxide (GO), Pt/WO_3 and Pt/WO_3-GO. GO was produced by Hummers' methods [10]. WO_3-GO was synthesized by one-pot synthesis with mixing surfactant, WO_3 and GO. Pt/WO_3 and Pt/WO_3-GO were synthesized by solvothermal process and dried at 110°C overnight. The TEM images of Pt/WO_3-GO showed the lumps of WO_3 obviously at various sizes. Also, the particle sizes of the Pt were up to 10 nm and WO_3's particle sizes were 20~50 nm. The result of the experiment showed that the photodegradation ability of mesoporous Pt/WO_3, WO_3-GO and Pt/WO_3-GO were much greater than bare WO_3. Especially, mesoporous Pt/WO_3-GO had 3, 2 and 1.15 times better photodegradation efficiency compared to mesoporous WO_3, WO_3-GO and Pt/WO_3, respectively. This improved efficiency is because of the GO sheets by helping free electrons to transfer easily. In another report, graphene oxide (GO), tungsten oxide ($W_{18}O_{49}$) nanowires, and tungsten oxide-reduced graphene oxide ($W_{18}O_{49}$-RGO) aerogel was used to compare the degradation of six organic dyes, Rhodamine B, reactive black 39, reactive yellow 145, weak acid black BR, methyl orange (MO), and weak acid yellow G[11]. GO was synthesized by a modified Hummers method. $W_{18}O_{49}$ nanowires and $W_{18}O_{49}$-RGO were synthesized by solvothermal process with heating them at 200°C for 12 hr. SEM and TEM images showed that the $W_{18}O_{49}$ samples were composed of several bundles of nanowires which looks like flowers. The diameters of nanowires were about 10~20 nm. The surface area, measured by BET, was 228 m^2/g and the pore volume, measured by BJH, was 0.50 cm^3/g. From the result of Photodegradation of MO under visible light, the $W_{18}O_{49}$-RGO showed significant photodegradation ability compared to RGO and $W_{18}O_{49}$. While bare $W_{18}O_{49}$ nanowire degraded 68% of MO, $W_{18}O_{49}$-RGO decomposed MO almost completely in 25 minutes. Finally, pure WO_3, multi-walled carbon nanotubes (MWCNTs) and multi-walled carbon nanotube/tungsten trioxide (MWCNT/WO_3) were used for the new photocatalysis of methylene blue (MB) dye under UV-Vis light[12]. For MWCNT, commercial material was used and MWCNT/WO_3 was synthesized by solvothermal process. From the FE-SEM image, the surface of MWCNT were magnified. The diameter of MWCNTs was measured as 15~30 nm and the spherical WO_3 particles were shown on planar WO_3 and tubular MWCNTs. The TEM showed the circular WO_3 and tubular MWCNTs. The result showed the pure MWCNTs had poor photodegradation ability. Unlike MWCNTs, hybrid photocatalyst, MWCNT/WO_3, showed better photodegradation efficiency. This is because of the larger surface area, isolation of electron/hole pairs and high oxidation ability. Therefore, 2% of MWCNT/WO_3 showed the most efficient photodegradation ability.

2.3. Metal oxide nanocomposites

Adding TiO_2 on WO_3 can increase the device life time five times compared to pure WO_3, with the side effect of lowering the coloration efficiency[13]. Here, thin films of tungsten oxide doped with titanium (Ti : WO_3) were made to prepare dendrite shaped surfaces using reactive co-sputtering of titanium and tungsten in an argon and oxygen atmosphere. Films synthesized at different oxygen flow rates was conducted for pressures of 1.0×10^{-3}, 2.0×10^{-3}, 3.0×10^{-3}, 4.0×10^{-3}, 5.0×10^{-3} mbar. With the metastable phase of hexagonal WO_3 being the dominant phase at all pressures, the ratio of the stable phase of monoclinic WO_3 is increased as the pressure of oxygen chamber is increased. Unlike pure tungsten oxide, annealed Ti : WO_3 exhibits a dendrite pattern on the surface, which decreases in size and density as the pressure of oxygen is raised. This is because Heating the substrate during

the deposition process forms Ti : WO_3 seed particles and annealing causes free energies of the planes in the crystal to change, resulting in a difference in relative growth between planes. Electrochemical reversibility, optical modulation, and coloration efficiency all increased with increasing oxygen pressure for the Ti : WO_3 thin films. The degrading of methylene blue was also higher for Ti : WO_3 than plain WO_3 (because the heterojunction allows charge carriers to be transferred between TiO_2 and WO_3), and efficiency increased with increasing oxygen pressure. The efficiency of both electrochromism and photocatalysis is positively affected by the increase in surface area, each attributed to enhanced intercalation/de-intercalation and increased generation of electron-hole pairs/hole consumption leading to increased formation of the OH· radicals, respectively. In another report Fe_2O_3@WO_3 with 0D Fe_2O_3 on 3D WO_3 is synthesized in a relatively simple method by mixing $Na_2WO_4 \cdot 2H_2O$, citric acid dissolved in water with an aqueous HCl solution, heating at 120°C for 24 h, and then calcinating at 400°C for 4 h[3]. Then the WO_3 was mixed with $Fe(NO_3)_3 \cdot 9H_2O$ solution and calcinated at 400°C for 4 h to get the desired result. XPS and XRD both confirms the iron oxide coupled with WO_3 is Fe_2O_3. Pure WO_3 has a monoclinic structure while pure Fe_2O_3 has a rhombohedral structure. FESEM shows the WO_3 structure is maintained while iron oxide is distributed on it. RhB has an alkaline character which makes adsorption of RhB is weaker for Fe_2O_3@WO_3 (28%) than for pure WO_3 (42%) (Fig. 2). The photocatalytic degradation, on the other hand, is accelerated. When H_2O_2 is added to the solution, degradation is improved further. In the case of 5 mM H_2O_2, 85.7% of RhB was degraded after 45 min. While increasing the temperature that $Fe(OH)_3$ is calcinated on WO_3 raises adsorption of RhB, the degradation of RhB rises only at first, due to the increase in crystallinity affecting the transfer of electron-hole pairs, then decreases after the optimum temperature of 400°C as Fe_2O_3 nanoparticles agglomerate and cause a decrease in surface area. RhB degradation in the visible-light photocatalytic reaction by Fe_2O_3@WO_3 is enhanced as concentration of H_2O_2 is increased, for up to 5 mM H_2O_2 concentration, as it helps initiate the reaction by consuming the photogenerated electrons. Taking away this difference caused by H_2O_2 concentration, the activity of Fe_2O_3@WO_3 is increased 68% compared to pure WO_3 when at the optimum value of 1% Fe_2O_3. Anything higher would result in agglomerates decreasing surface area and thus the active sites. Fe_2O_3@WO_3 showed a high recyclability by going through five, 75 minute cycles with only a slight drop in degradation efficiency. Xi *et al.* reported synthesis of Fe_3O_4/WO_3 with a hierarchical core-shell structure. It was prepared by solvothermal process in presence of binary oleic acid-ethylene glycol (EG) mixture and dispersed in a solution containing anhydrous ethanol, EG, and WCl_6 which is heated at 180°C for 24 h to get $W_{18}O_{49}$ nanocrystals[14]. SEM and TEM images show nanoparticles about 5~10 nm in size form uniform Fe_3O_4 microspheres of diameter 450 nm. Leaf-like $W_{18}O_{49}$ nanoplates of 10~20 nm thickness surround their surfaces in a radial direction. XRD patterns show the composite contains monoclinic-phase $W_{18}O_{49}$ with spinel-phase of Fe_3O_4. BET calculations showed specific surface area was 34 m^2/g. Using a Barrett-Joyner-Halenda method, it was observed that mesopores and macropores of diameter 3~20 nm were each constructed from Fe_3O_4 and WO_3, respectively. Fe_3O_4/WO_3 core-shell structured photocatalysts showed higher photodegradation for RhB and methylene blue than WO_3 hollow microspheres, with RhB being almost fully degraded by Fe_3O_4/WO_3 after irradiation of visible light for 1.5 h. Using a superconducting quantum interference device magnetometer (SQIDM) ferromagnetic behavior is observed. The highly stable structure of Fe_3O_4/WO_3 lets it be recycled without decrease in photocatalytic activity three times.

In another report $W_{18}O_{49}$ was synthesized from alcoholysis of WC_{16} in a solvothermal process where heat was applied for 24 h at 160°C[15]. The mixing with TiO_2 resulted in a $W_{18}O_{49}/TiO_2$ hybrid, creating a charge-transfer pathway. Using SEM and TEM, urchin-like $W_{18}O_{49}$ formed from nanowires of length 500~600 nm

and diameters of < 20 nm. Images from HRTEM shows the $W_{18}O_{49}$ nanowires are monocrystalline. XRD shows that $W_{18}O_{49}$ and WO_3 is each in the monoclinic phase. $W_{18}O_{49}$ and WO_3 shows urchin-like structure and large BET surface are of 178, and 169 m^2g^{-1} each. With visible light photodegradation of MO and phenol, there is a negligible amount of degradation activity by TiO_2. $W_{18}O_{49}$ (90 wt%)/TiO_2 has best photocatalytic efficiency than pure $W_{18}O_{49}$ for the degradation of methyl orange (MO). Due to the fact that energy levels of the two semiconductors are similar, charge transfer on the interfaces of the two is easy, resulting in better charge separation. Oxygen defects in the $W_{18}O_{49}$ structure are important for the hybrids because they give $W_{18}O_{49}$ an advantage in the reduction activity of CO_2 compared to WO_3.

2.4. Mixed metal oxide nanocomposite

WO_3, ZnS nanoparticles (NPs), 20 wt% ZnS-WO_3 and 40 wt% ZnS-WO_3 were used to compare the degradation efficiency of methylene blue (MB) dye under UV-Vis light[16]. WO_3 nanosheets, ZnS NPs and ZnS-WO_3 nanosheet were synthesized by hydrothermal method, precipitation method and wet impregnation method, respectively. The HRTEM images showed the morphology of WO_3. It represented WO_3 as a sheet of paper and the ZnS NPs were embedded on it. 20 wt% ZnS-WO_3 showed the highest photodegradation efficiency compared to WO_3, ZnS NPs and 20 wt% ZnS-WO_3. The photodegradation efficiencies under UV-Vis light after 240 minutes were 68.17, 75.79, 68.74 and 92.40% for ZnS NPs, WO_3 nanosheet, 40 and 20 wt% ZnS-WO_3. Low efficiency of 40 wt% ZnS-WO_3 was expected to be covering the surface of WO_3 nanosheets with ZnS NPs and interrupting photons to reach the WO_3 nanosheets. In another report, various concentration of Sn-WO_3/g-C_3N_4 were used to compare the photodegradation efficiency of anionic methyl orange (MO) and cationic Rhodamine B (Rh B) to bare WO_3, Sn-WO_3, g-C_3N_4 and 8% WO_3/g-C_3N_4 under visible light[17]. Sn-WO_3 solid solution and g-C_3N_4 were synthesized by solvothermal method and calcination method, respectively. WO_3/g-C_3N_4 and Sn-WO_3/g-C_3N_4 were synthesized by calcination method. The SEM image of Sn-WO_3/g-C_3N_4 showed Sn-WO_3 nanoparticles were dispersed over the g-C_3N_4 sheet. The photocatalysis were conducted with 87% of MO during 120 minutes and 99% of Rh B during 50 minutes under visible light. The result showed 8% of Sn-WO_3/g-C_3N_4 had the highest photodegradation effi- ciency. Sn-WO_3 and g-C_3N_4 had poor photodegradation efficiency and WO_3/g-C_3N_4 showed better efficiency than previous two materials.

Another group compared pure $BiFeO_3$, pure Bi_2WO_6 and $BiFeO_3$-Bi_2WO_6 for photodegradation efficiency of methylene blue (MB) and Rhodamine B (Rh B) under visible light irradiation[18]. $BiFeO_2$ particles were synthesized by solvothermal method dried at 80°C for 24 h. Pure Bi_2WO_6 was synthesized by hydrothermal method. $BiFeO_3$-Bi_2WO_6 nanocomposites were synthesized by solvothermal method with 1 : 1 mol ratio. The TEM image showed the size, morphology and lattice fringe of three materials. In the TEM image, the pure $BiFeO_3$ was a 25~50 nm length rectangular and Bi_2WO_6 was about 50~100 nm plate. $BiFeO_3$-Bi_2WO_6 had both $BiFeO_6$ and Bi_2WO_6 morphology. BET method measured the surface area of the materials. The surface area of $BiFeO_3$ was largest with 8.44 m^2g^{-1} and the surface areas of $BiFeO_3$-Bi_2WO_6 were small in general. The most efficient photocatalyst was 1 : 1 mol ratio of in both MB and Rh B solutions. After 75 minutes of photodegradation under visible light, $BiFeO_3$-Bi_2WO_6 decomposed MB and Rh B 54 and 36%, respectively. The pure $BiFeO_3$ and Bi_2WO_6 showed poor efficiency compared to $BiFeO_3$-Bi_2WO_6. Although $BiFeO_3$ had the largest surface area, it showed the lowest photodegradation efficiency. It was predicted as the $BiFeO_6$ and Bi_2WO_6 had synergetic effect together by isolating electrons and holes. Ngigi *et al.* used CdS-WO_3 to compare the photodegradation efficiency of Ethylparaben under visible light with bare WO_3[19]. CdS-WO_3 nanocomposite was synthesized by hydrothermal process. SEM image showed the lump of square WO_3 nanoparticles and it was shown in TEM image, too. TEM

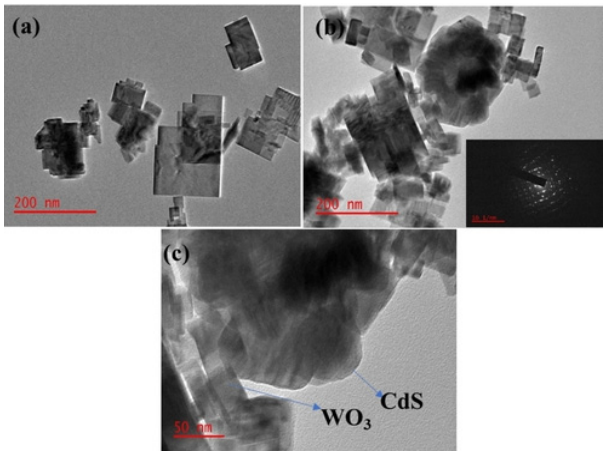

Fig. 3. TEM images of (a) WO_3, (b) CdS-WO_3 3 : 7 (inset SAED), and (c) high magnification of the nanocomposite (Reproduced from Ngigi *et al.*, 19 with permission of Wiley).

image showed that the spherical CdS nanoparticles were on the square WO_3 structure (Fig. 3). The CdS-WO_3 with the ratio of 3 : 7 showed the most efficient photodegradation compared to the CdS-WO_3 with the ratio of 1 : 1.

In another study, fly ash (FAw) and tungsten oxide-fly ash oxide ($FAWO_3$) were used to compare the photodegradation efficiency of bemacid blau (BB), bemacid rot (BR) and a heavy metal (ion-Cu^{2+})[20]. Raw fly ash was collected from the electro-filter the plant and WO_3 was commercial material. Tungsten oxide-fly ash oxide was synthesized by hydrothermal process. From the SEM images, the surface of FAw showed the rough surface with many pores on it. However, $FAWO_3$ showed smooth surface and uniformly dispersed pores because of the hydrothermal process. This experiment showed better photocatalytic efficiency with the novel composites. The novel nanocomposite showed better removal efficiency in combined adsorption and photocatalysis process.

3. Conclusions

WO_3 is a major interest in the area of degrading organic dyes using photocatalysis. Although changing the morphology of pure tungsten oxide can improve degradation efficiency by increasing surface area with 3D structures while at the same time improving charge transport with 1D structures, it has its limits. This is due to the energy level of the conduction band being higher than the O_2/O_2^- reduction potential. This can be made up for by using a co-catalyst. Possible co-catalysts include noble metals such as Pt, Ag, Au, out of which Pt is focused in this review for it is the most commonly used. These co-catalysts act as an electron pool to facilitate the reduction of oxygen. The disadvantage of this methods is that these noble metals are expensive. This has led to the introduction of other less-expensive methods of increasing the efficiency of tungsten oxide. First, by coupling with metal oxide semiconductors such as Fe_2O_3 or TiO_2. Second, by using carbon composites such as graphene, thus increasing interfacial charge transfer. Nanodiamond-loaded tungsten oxide goes further by being transparent as well as showing high charge transfer qualities. Combining the different methods is also used to try to combine the advantages behaviors of each method, with the disadvantage that doing so will increase the number of procedures spent on preparation of the complex photocatalyst. The development of photocatalysis is related to membrane photoreactor and integration of photocatalysis with water purification membrane process.

Reference

1. S. G. Kumar and K. S. R. K. Rao, “Tungsten-based nanomaterials (WO_3 & Bi_2WO_6): Modifications related to charge carrier transfer mechanisms and photocatalytic applications”, *Appl. Surf. Sci.*, **355**, 939 (2015).
2. M. Pelaez, N. T. Nolan, S. C. Pillai, M. K. Seery, P. Falaras, A. G. Kontos, P. S. M. Dunlop, J. W. J. Hamilton, J. A. Byrne, K. O’Shea, M. H. Entezari, and D. D. Dionysiou, “A review on the visible light active titanium dioxide photocatalysts for environmental applications”, *Appl. Catal. B: Environ.*, **125**, 331 (2012).

3. S. Bai, K. Zhang, J. Sun, R. Luo, D. Li, and A. Chen, "Surface decoration of WO_3 architectures with Fe_2O_3 nanoparticles for visible-light-driven photocatalysis", *CrystEngComm*, **16**, 3289 (2014).
4. D. Xu, T. Jiang, D. Wang, L. Chen, L. Zhang, Z. Fu, L. Wang, and T. Xie, "pH-dependent assembly of tungsten oxide three-dimensional architectures and their application in photocatalysis", *ACS Appl. Mater. Interfaces*, **6**, 9321 (2014).
5. R. Abe, H. Takami, N. Murakami, and B. Ohtani, "Pristine simple oxides as visible light driven photocatalysts: Highly efficient decomposition of organic compounds over platinum-loaded tungsten oxide", *J. Am. Chem. Soc.*, **130**, 7780 (2008).
6. A. Purwanto, H. Widiyandari, T. Ogi, and K. Okuyama, "Role of particle size for platinum-loaded tungsten oxide nanoparticles during dye photodegradation under solar-simulated irradiation", *Catal. Commun.*, **12**, 525 (2011).
7. L. Xu, D. Gu, X. Chang, L. Chai, Z. Li, X. Jin, and S. Sun, "Adsorption and photocatalytic study of dye degradation over the g-C_3N_4/$W_{18}O_{49}$ nanocomposite", *Micro Nano Lett.*, **13**, 541 (2018).
8. H. I. Kim, H. N. Kim, S. H. Weon, G. H. Moon, J. H. Kim, and W. Y. Choi, "Robust co-catalytic performance of nanodiamonds loaded on WO_3 for the decomposition of volatile organic compounds under visible light", *ACS Catal.*, **6**, 8350 (2016).
9. L. Mei, H. Zhao, and B. Lu, "Ultra-efficient photocatalytic properties in porous tungsten oxide/graphene film under visible light irradiation", *Adv. Sci.*, **12**, 1500116 (2015).
10. A. A. Ismail, M. Faisal, and A. Al-Haddad, "Mesoporous WO_3-graphene photocatalyst for photocatalytic degradation of Methylene Blue dye under visible light illumination", *J. Environ. Sci.*, **66**, 328 (2018).
11. X. Li, S. Yang, J. Sun, P. He, X. Xu, and G. Ding, "Tungsten oxide nanowire-reduced graphene oxide aerogel for high-efficiency visible light photocatalysis", *Carbon*, **78**, 38 (2014).
12. M. Dinari, M. M. Momeni, and M. Ahangarpour, "Efficient degradation of methylene blue dye over tungsten trioxide/multi-walled carbon nanotube system as a novel photocatalyst", *Appl. Phys. A.*, **112**, 1 (2016).
13. A. Karuppasamy, "Electrochromism and photocatalysis in dendrite structured Ti : WO_3 thin films grown by sputtering", *Appl. Surf. Sci.*, **359**, 841 (2015).
14. G. Xi, B. Yue, J. Cao, and J. Ye, "Fe_3O_4/WO_3 hierarchical core-shell structure: High-performance and recyclable visible-light photocatalysis", *Chem.: Eur. J.*, **17**, 5145 (2011).
15. Z. F. Huang, J. J. Zou, L. Pan, S. Wang, X. Zhang, and L. Wang, "Synergetic promotion on photoactivity and stability of $W_{18}O_{49}$/TiO_2 hybrid", *Appl. Catal. B: Environ.*, **147**, 167 (2014).
16. G. Palanisamy, K. Bhuvaneswari, G. Bharathi, D. Nataraj, and T. Pazhanivel, "Enhanced photocatalytic properties of ZnS-WO_3 nanosheet hybrid under visible light irradiation", *ChemistrySelect*, **32**, 9422 (2018).
17. K. E. Ahmed, D. H. Kuo, M. A. Zeleke, O. A. Zelekew, and A. K. Abay, "Synthesis of Sn-WO_3/g-C_3N_4 composites with surface activated oxygen for visible light degradation of dyes", *J. Photochem. Photobiol.*, **369**, 133 (2019).
18. S. Chaiwichian, K. Wetchakun, W. Kangwansupamonkon, and N. Wetchakun, "Novel visible-light-driven $BiFeO_3$-Bi_2WO_6 nanocomposites toward degradation of dyes", *J. Photochem. Photobiol. A*, **349**, 183 (2017).
19. E. M. Ngigi, E. M. Kiarii, P. N. Nomngongo, and C. J. Ngila, "Application of Z-Scheme CdS WO_3 nanocomposite for photodegradation of ethylparaben under irradiation with visible light: A combined experimental and theoretical study", *ChemistrySelect*, **34**, 9845 (2018).
20. M. Visa, C. Bogatu, and A. Duta, "Tungsten oxide - fly ash oxide composites in adsorption and photocatalysis", *J. Hazard. Mater.*, **289**, 244 (2015).